Inorg. Chem. **2008**, *47*, 6303−6313

Hydrogen Absorption in Transition Metal Silicides: La_3Pd_5Si-Hydrogen System

Yaroslav O. Tokaychuk,*,†,‡ Yaroslav E. Filinchuk,†,§ Denis V. Sheptyakov,⊥ and Klaus Yvon†

Laboratory of Crystallography, University of Geneva, 24 quai Ernest Ansermet, CH-1211 Geneva, Switzerland, Swiss-Norwegian Beam Lines, European Synchrotron Radiation Facility, 6 rue Jules Horowitz, 38043 Grenoble, France, and Laboratory for Neutron Scattering, ETH Zurich & Paul Scherrer Institut, CH-5232 Villigen PSI, Switzerland

Received February 28, 2008

Pressure-composition isotherm measurements show that the ternary lanthanum palladium silicide phase La_3Pd_5Si absorbs reversibly up to 5 hydrogen atoms per formula unit at 550 K and 14 bar hydrogen pressure. *In-situ* synchrotron and neutron powder diffraction reveals three phases, an α-phase having the limiting composition $La_3Pd_5SiD_{\sim 1.6}$ at low deuterium pressure (at up to 9.5 bar D_2 and 550 K), a β-phase $La_3Pd_5SiD_{\sim 2.30-4}$ at intermediate deuterium pressure (<9.5 bar D_2 and 550 K), and a relatively unstable γ-phase $La_3Pd_5SiD_{\sim 5}$ at high deuterium pressure (obtained at 75 bar D_2 and 293 K). While the α and β phases retain the symmetry of the H-free La_3Pd_5Si (space group *Imma*), the γ-phase undergoes a symmetry lowering ($a_\gamma \sim a_\beta$, $b_\gamma \sim 3b_\beta$ and $c_\gamma \sim c_\beta$, $V_\gamma \sim 3V_\beta$, space group *Pmnb*). The structure of the α-phase contains isolated [Pd−D−Pd] fragments, which are joined into polymeric $(-Pd-D-Pd-)_n$ *zig-zag* chains in the β-phase. In the γ-phase some D sites depopulate, while new D sites are occupied, thus leading to a partial interruption of the *zig-zag* chains and the formation of isolated [D−Pd−D−Pd] and [D−Pd−D−Pd−D] fragments. This unexpected behavior can be attributed to the onset of repulsive Si−D and D−D interactions (Si−D > 3.0 Å, D−D > 2.1 Å) that divide the structure into Si-poor slabs that absorb hydrogen and Si-rich slabs that do not. The competition between silicon and deuterium which act as a transition metal ligand is further underlined by the fact that Pd atoms having one Si ligand are capable of forming Pd−D bonds, whereas Pd atoms having two Si ligands are not.

Introduction

Only few solid-state metal silicides have been studied so far with respect to their hydrogenation behavior. This is likely because silicon is generally perceived as an unfavorable element for improving hydrogenation properties of hydrogen storage materials, in particular of transition metal compounds. In fact, the great majority of *d*-metal silicides investigated so far show rather poor hydrogen capacities under technically feasible conditions, and this is at least partially attributed to the existence of repulsive interactions between silicon and hydrogen in their solid state structures.[1] In hydrogenated Pd_9Si_2,[2,3] for example, hydrogen avoids short contacts with silicon by filling pyramidal Pd_5 interstices. Yet, recent work on *p*-metal silicides has shown some interesting results. The ternary silicide SrAlSi, for example, reacts with hydrogen under relatively severe conditions (50 bar and 600−700°C), thus leading to a stoichiometric "Zintl phase" hydride of composition SrAlSiH.[4] The hydride is relatively stable (hydrogen desorption temperature above 600°C under 1 bar argon pressure) and contains two-dimensional polyanion $[AlHSi]^{2-}$ composed of three-bonded $[Al-H]^-$ and Si^-

* To whom correspondence should be addressed. E-mail: tokaychuk@mail.lviv.ua.
† University of Geneva.
‡ Present address: Chimie Métallurgique des Terres Rares, Institut de Chimie et des Matériaux Paris-Est CNRS UMR 7182, 2−8 rue Henri Dunant 94320 Thiais, France.
§ European Synchrotron Radiation Facility.
⊥ Paul Scherrer Institut.

(1) Rundqvist, S.; Tellgren, R.; Andersson, Y. *J. Less-Common Met.* **1984**, *101*, 145–168.
(2) Udovic, T.J.; Rush, J. J.; Flanagan, T. B.; Noh, H.; Andersson, Y. *J. Alloys Compd.* **1997**, *253−254*, 255–257.
(3) Karmonik, C.; Udovic, T. J.; Huang, Q.; Rush, J. J.; Andersson, Y.; Flanagan, T. B. *Physica B* **1998**, *241−243*, 332–334.
(4) Björling, T.; Noréus, D.; Jansson, K.; Andersson, M.; Leonova, E.; Edén, M.; Hålenius, U.; Häussermann, U. *Angew. Chem., Int. Ed.* **2005**, *44*, 7269–7273.

10.1021/ic800382x CCC: $40.75
Published on Web 06/07/2008

entities that are charge balanced by Sr^{2+}. Interestingly, the Si and Al atoms in the hydride are ordered, in contrast to the starting material SrAlSi in which they are disordered (AlB_2 type). This hydrogen-induced ordering of Al/Si atoms is presumably due to the selective bonding of D to Al (d_{Al-D} = 1.77 Å) at the expense of Si (shortest Si−H distance is 3.38 Å). While this result confirms that Si and H repel each other in that structure, in marked contrast to silanes, it shows that such repulsions do not necessarily prevent hydrogen absorption altogether. Another recent example is the ternary silicide deuteride Li_4Si_2D.[5] The compound was prepared by ball milling LiD and Si, evacuation at 773 K, and subsequent deuteration at 0.7 MPa of D_2 at 723 K. Its structure displays deuterium centered Li_6 octahedra in which D atoms avoid the Si−Si chains. A similar situation prevails in the rather stable silicides $AE_5Si_3H_2$ (AE = Ca, Sr, Ba, Eu). They crystallize with a filled Cr_5B_3-type structure in which AE_4 tetrahedra are occupied by hydrogen thus avoiding silicon (d_{Si-H} = 3.95 Å).[6] Finally, the binary silicide CaSi is known to absorb hydrogen reversibly at relatively mild conditions (473−573 K; 9 MPa) to a limiting composition of $CaSiH_{1.3}$.[7] Its CrB-type derivative structure displays a relatively large fraction of long Si−H distances (3.04−3.95 Å from structure refinement, 3.08−4.01 Å from theoretical calculations) while some Si−H distances are relatively short (Si−H = 1.85 Å from structure refinement, 1.58 Å from theoretical calculations). This suggests that Si−H bond formation similar to silanes may be feasible in solid state metal hydrides under certain conditions.

Here, we report on the hydrogenation properties of the ternary *d*-metal silicide La_3Pd_5Si.[8] The compound crystallizes with an ordered, orthorhombic Ce_3Pd_5Si type structure (space group *Imma*, 36 atoms per unit cell)[9] that displays five symmetry independent atom sites (2 La, 2 Pd, 1 Si). It will be shown that the compound absorbs hydrogen under relatively mild conditions by forming three distinct hydride phases whose host structures contain up to 18 symmetry independent atom sites (9 Pd, 6 La, 3 Si) and up to 8 different types of metal interstices that are nearly fully occupied by hydrogen. As far as we know, this silicide system is the most complex investigated so far with respect to hydrogenation properties. The results presented below not only confirm the influence of repulsive Si−H and H−H interactions in its structure but also reveal the competition between silicon and deuterium acting as transition metal ligands, at least at the temperature/pressure conditions investigated.

Experimental Section

Synthesis and Preliminary X-ray Diffraction Experiments. Starting materials for the alloys' synthesis were La pieces (Aldrich, 99.9%), Pd bulk (99.9+%), and Si pieces (Aldrich, m6N). The elements were weighted in stoichiometric ratios and arc-melted under a purified argon atmosphere. To ensure homogeneity each sample was remelted three times with nearly no mass losses. X-ray powder patterns of the as-cast alloys collected on the laboratory diffractometer Bruker D8 (Cu $K_{\alpha 1}$ radiation) indicated a single La_3Pd_5Si phase with a Ce_3Pd_5Si-type structure (space group *Imma*) and lattice parameters a = 13.1490(6), b = 7.4394(3), c = 7.6567(3) Å, and V = 748.98(6) Å^3, which are in good agreement with ref 8. Hydrogenation (H_2 gas, 99.9999%, Alphagas) and deuteration (D_2 gas, 99.8%, AGA) were carried out in high-temperature high-pressure autoclaves. Five different hydrogenated or deuterated samples were synthesized under various conditions (273−473 K, 75−150 bar H_2/D_2). Obtained hydrides and deuterides were dark-gray and more brittle than the initial La_3Pd_5Si alloy, probably because of some strains introduced during the hydrogenation. The hydrogenated and deuterated samples were stable with respect to oxidation and reaction with moisture, but they completely desorb hydrogen/deuterium during a few days.

Structure Characterization by Synchrotron and Neutron Powder Diffraction. Room temperature synchrotron powder diffraction experiments were carried out at the Swiss-Norwegian Beam Lines (SNBL) at ESRF (Grenoble, France) using the wavelengths λ = 0.59954(1) Å or 0.52014(1) Å (just above the Pd K-absorption edge at 0.50915 Å), Debye-Scherrer geometry, 2θ range 3.5−50.5° with step size 0.004−0.007°. The wavelengths and zero-shifts were refined from a standard Si sample. High-resolution neutron powder diffraction data on deuterides were collected *ex-situ* on the diffractometer HRPT at SINQ (PSI, Villigen, Switzerland) using the wavelengths 1.493814(1) Å, 1.372060(1) Å, or 1.372000(1) Å, 2θ range 4.5−164.5° with step size 0.1°, and data collection time ~7−9 h per pattern. The wavelengths and zero-shifts were refined from a standard $Na_2Ca_3Al_2F_{14}$ (NAC) sample.

All diffraction profile and structure refinements were performed using the FULLPROF SUITE software.[10] As a starting model of the metal substructures in α and β phases the atomic parameters of La_3Pd_5Si were used. The structure of α-$La_3Pd_5SiD_{1.44(3)}$ (a solid solution of deuterium in the parent intermetallic phase) was refined from the neutron powder data collected at room temperature on the deuteride obtained during an *in-situ* diffraction experiment (for the details see below). The sample contained two phases: α-$La_3Pd_5SiD_{1.44(3)}$ (60.7(5) wt %, a = 13.3342(11), b = 7.5479(5), c = 7.6995(7) Å, V = 774.92(11) Å^3) and β-$La_3Pd_5SiD_x$ (39.3(4) wt %, a = 12.8886(14), b = 7.6530(8), c = 8.3075(8) Å, V = 819.42(15) Å^3). In the first step the metal atoms positions were fixed as in La_3Pd_5Si and one deuterium atom site was located using the program FOX.[11] At the second step all profile and structural parameters for the main α-phase were refined by the Rietveld method. The background was defined using a Fourier filtering technique with a window of 50°. High resolution synchrotron data did not show any distortion of the orthorhombic cell for β-phase but revealed an anisotropic peak broadening typical for hydrides with anisotropically expanded unit cell. The metal atoms positions in β-$La_3Pd_5SiH_x$ were refined using two synchrotron powder patterns collected at room temperature for its lower and upper limits

(5) Wu, H.; Hartman, M. R.; Udovic, T. J.; Rush, J. J.; Zhou, W.; Bowman, R. C., Jr.; Vajo, J. J. *Acta Crystallogr.* **2007**, *B63*, 63–68.
(6) Leon-Escamilla, E. A.; Corbett, J. D. *J. Solid State Chem.* **2001**, *159*, 149–162.
(7) (a) Ohba, N.; Aoki, M.; Norikate, T.; Miwa, K.; Towata, S. *R&D Rev. Toyota CRDL* **2004**, *39*, 40–45. (b) Aoki, M.; Ohba, N.; Norikate, T.; Towata, S. *Appl. Phys. Lett.* **2004**, *85*, 387–388. (c) Aoki, M.; Ohba, N.; Norikate, T.; Towata, S. *J. Alloys Compd.* **2005**, *404−406*, 402–404. (d) Ohba, N.; Aoki, M.; Norikate, T.; Miwa, K.; Towata, S. *Phys. Rev. B* **2005**, *72*, 075104.
(8) Malik, S. K.; Kundaliya, D. C. *Solid State Commun.* **2003**, *127*, 279–282.
(9) Gribanov, A. V.; Seropegin, Yu., D.; Kubarev, O. L.; Akselrud, L. G.; Bodak, O. I. *J. Alloys Compd.* **2001**, *317−318*, 324–326.
(10) Rodriguez-Carvajal, J. *FULLPROF SUITE*; LLB Saclay & LCSIM: Rennes, France, 2003.
(11) Favre-Nicolin, V.; Cerný, R. *J. Appl. Crystallogr.* **2002**, *35*, 734–743.

Table 1. Results of the *in-Situ* NPD upon Deuterium Absorption by La_3Pd_5Si at 560 K

no.	D_2 pressure	phase (refined D-content)	phase content, %	*a*, Å	*b*, Å	*c*, Å	*V*, Å^3
1	dynamic vacuum	α-$La_3Pd_5SiD_{0.31(5)}$	100	13.232(3)	7.4717(11)	7.7092(16)	762.2(3)
2	small portions of D_2 gas were let in	α-$La_3Pd_5SiD_{0.50(3)}$	100	13.268(2)	7.4909(8)	7.7221(12)	767.5(2)
3		α-$La_3Pd_5SiD_{0.69(3)}$	100	13.299(2)	7.5124(8)	7.7350(12)	772.8(2)
4		α-$La_3Pd_5SiD_{0.81(3)}$	100	13.314(3)	7.5246(8)	7.7415(13)	775.6(2)
5		α-$La_3Pd_5SiD_{0.94(3)}$	100	13.333(3)	7.5436(9)	7.7556(14)	780.0(2)
6	3.0 bar	α-$La_3Pd_5SiD_{1.02(3)}$	100	13.338(3)	7.5536(9)	7.7651(14)	782.4(2)
7	5.0 bar	α-$La_3Pd_5SiD_{1.06(3)}$	100	13.345(3)	7.5654(10)	7.7788(13)	785.4(2)
8	7.0 bar	α-$La_3Pd_5SiD_{1.14(3)}$	100	13.343(3)	7.5827(11)	7.8018(13)	789.4(2)
9	9.5 bar	α-$La_3Pd_5SiD_{1.6}$	39	13.261(10)	7.638(5)	7.916(4)	801.8(9)
		β-$La_3Pd_5SiD_{2.30(8)}$	61	13.193(6)	7.648(3)	8.076(3)	814.8(6)
10	12.5 bar	β-$La_3Pd_5SiD_{2.71(5)}$	100	13.102(2)	7.6734(14)	8.1680(16)	821.2(3)

of hydrogen concentration. Two deuterium atom positions in the structure of the β-phase (lower concentration limit) were located by using the *ex-situ* neutron data and the program FOX.

One of the samples was unloaded from an autoclave containing 75 bar of hydrogen pressure immediately before a synchrotron diffraction experiment. A rapid measurement at SNBL, using the detector with analyzer crystals, revealed that besides the main β-$La_3Pd_5SiH_x$ phase (91 wt %) the sample contains a new high-pressure γ-$La_3Pd_5SiH_x$ (8 wt %). The peaks from the second phase disappeared rapidly (∼ 10 min.) because of fast hydrogen desorption from the sample. The crystal structure determination for the H(D)-rich γ-phase was done in two steps. In the first step, the metal atom substructure has been determined from high-resolution synchrotron powder data. They were collected on the sample freshly loaded with deuterium (75 bar) using a fast strip detector at the Materials Science Beam Line at SLS. One complete powder pattern has been collected in 10 s, using the wavelength of 0.70832(1) Å, Debye-Scherrer geometry, resulting in the data in the 2θ range 4.5−50.5° with step size 0.0037°. The pattern has been modeled with a structure of the intermetallic compound having a larger unit cell volume, but some small peaks indicated a possible superstructure. These peaks have been indexed by tripling the *b* parameter. Thus, the relations between the unit cell parameters for the γ- and β-hydride are as follows: $a_\gamma \sim a_\beta$, $b_\gamma \sim 3b_\beta$, $c_\gamma \sim c_\beta$, and $V_\gamma \sim 3V_\beta$. Such 3-fold superstructure along *b* of an *Imma* structure corresponds to an isomorphic subgroup *Imma*. In the next stage, only direct subgroups of *Imma* (tripled cell) were considered: four orthorhombic *I*-centered and eight orthorhombic *P*-centered space groups. Superstructure lines are very weak compared to the main peaks. However, their existence violates the *I*-centering and the *a* glide plane perpendicular to the *c*-axis. Among the four remaining direct subgroups of *Imma* (*Pnnb*, *Pnmb*, *Pmnb* and *Pmmb*), the most stable refinements for metal atom substructures, using synchrotron data only, were obtained in *Pnmb* and *Pmnb*. The solution of D-atom positions from neutron data was successful only in the space group *Pnmb*. The reliable full-matrix full profile Rietveld refinement of all structural and profile parameters in the space group *Pnmb* confirms the validity of our choice. Positional parameters for all metal atoms were transformed from the space group *Imma* to *Pmnb* by the program POWDER CELL[12] and refined with FULLPROF. The structure with the tripled unit cell contains 18 metal atoms in the asymmetric unit. In the second step, deuterium atoms positions were determined from neutron data. To obtain a neutron powder pattern on the high-deuterium pressure γ-phase, the deuteride was transported to PSI in an autoclave under 150 bar of D_2. There, it was slowly cooled over 2 weeks to 90 K. Then the autoclave was quickly opened and the sample was refilled into a V-cylinder within 2 min, immediately frozen in an Orange cryostat, and a high-resolution neutron powder pattern was collected at HRPT at 125 K. Eight deuterium atoms were located from the neutron data using the program FOX, fixing the coordinates of the metal atoms to those refined from the synchrotron data. The result was verified by analyzing the difference nuclear Fourier maps. Because of the very high complexity of the neutron pattern, the refinement of the profile parameters and the solution of the deuterium atoms' substructure were done iteratively. In the final refinement cycles, 87 profile and structural parameters were refined by the Rietveld method: 1 scale factor, 3 cell parameters, 4 profile parameters (Pseudo-Voigt peak shape function), 69 atomic coordinates, 1 overall isotropic displacement parameter, and 8 occupancy parameters for D-atoms. Soft restraints were applied to some Pd−Si and Pd−D distances: $d_{Pd1-Si2}$, $d_{Pd1-Si3}$, $d_{Pd2-Si1}$, $d_{Pd2-Si3}$, $d_{Pd3-Si1}$, $d_{Pd3-Si2}$, $d_{Pd5-Si2}$, $d_{Pd6-Si1}$, and $d_{Pd9-Si3}$ were restrained to 2.45(2) Å, and d_{Pd5-D4}, d_{Pd6-D5}, and d_{Pd8-D6} were restrained to 1.70(2) Å. The background was defined by a Fourier filtering technique with a window of 50°.

***In-Situ* Neutron Powder Diffraction.** Diffraction experiments during absorption and desorption of deuterium were carried out at the diffractometer DMC at SINQ (PSI). The main aim of these investigations was to monitor the phase transitions in the $La_3Pd_5Si-D_2$ system, determine the limits of deuterium concentration for different phases, and analyze the occupation of deuterium atoms as a function of D-concentration. A ∼5 g quantity of γ-$La_3Pd_5SiD_x$, stored under high D-pressure (100 bar) before the diffraction experiment, was loaded into a cylindrical stainless steel container of 9 mm inner diameter and was placed into a furnace installed at the DMC diffractometer. The system was connected to a deuterium pressure line, and *in-situ* desorption time-resolved NPD patterns were collected at room temperature. Diffraction data were collected with the wavelength of 2.5687(1) Å in the 2θ range 15−100° with step size 0.2°. An averaged time to collect one pattern was 10−30 min. When the spontaneous desorption at room temperature became slower, the sample was slowly heated up to 560 K. At the end of the desorption experiment a dynamic vacuum has been applied. In total, 46 patterns were collected during the desorption experiment.

An *in-situ* deuterium absorption experiment was done using the sample, desorbed at 560 K in the dynamic vacuum. The same temperature, 560 K, was set as a target point throughout the absorption experiment, while the actual temperature of the sample was precisely monitored. The first powder pattern showed that the sample is a single phase α-$La_3Pd_5SiD_x$. Deuterium gas was then added by small portions at increasing pressures (see Table 1). Each portion was immediately absorbed by the sample, resulting in a sharp increase of the sample temperature by ∼10−20 K within a few seconds. After adding a portion of D_2, the sample was kept at 560 K for ∼30−40 min to reach thermal and chemical equilibrium, and neutron diffraction patterns were collected during 2 h each using the wavelength $\lambda = 2.5687(1)$ Å, Debye-Scherrer geometry, and 2θ range of 19−100° with step size 0.1°. The maximum pressure

(12) Kraus, W.; Nolze, G. *J. Appl. Crystallogr.* **1996**, *29*, 301–303.

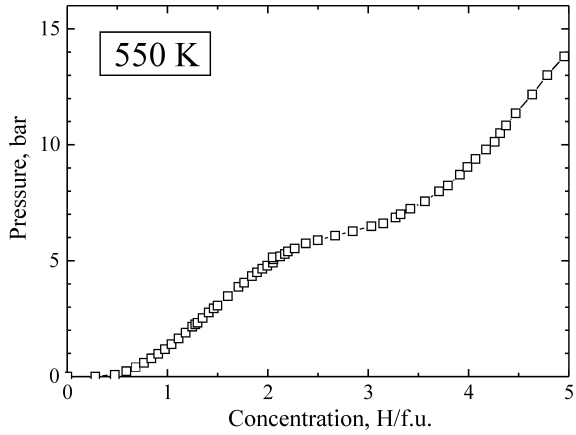

Figure 1. Pressure-Composition isotherm upon the hydrogen absorption by La_3Pd_5Si at 550 K.

reached was 12.5 bar. In total 10 powder patterns were collected during the deuterium absorption experiment.

Three phases were observed during the desorption experiment: deuterium-rich γ-$La_3Pd_5SiD_x$, intermediate β-$La_3Pd_5SiD_x$, and the solid solution of deuterium in the parent intermetallic phase, α-$La_3Pd_5SiD_x$. During the *in-situ* absorption experiment only two phases were observed: α-$La_3Pd_5SiD_x$ and β-$La_3Pd_5SiD_x$. The high-pressure γ-phase could not be reached in the experimentally accessible pressure range. The corresponding two-phase regions were clearly visible. All powder patterns collected during deuterium desorption were treated in the following way. For each phase the scale factor, four profile and three cell parameters were refined. Structural models for all phases as derived from the previous *ex-situ* high-resolution neutron and synchrotron diffraction experiments were used. Neutron patterns collected upon deuterium absorption were of much better quality (because of longer counting time). That allowed refining the D-sites' occupancies along with a scale factor, four profile and three cell parameters for each phase. Diffraction peaks from the *fcc* phase of the steel container were modeled by using six parameters. The background was approximated by a polynomial and 4−5 refined coefficients. A summary of the refinement results is presented in Table 1. The D-site occupancy for α-$La_3Pd_5SiD_x$ in the two-phase sample ($x = 1.6$ D/f.u., No. 9 in Table 1) was not refined but extrapolated from a linear dependency of the unit cell volume on the D-content: $V = 753.9(4) + 27.0(6)x$.

PCT Measurements. Pressure-Composition (P−C) isotherms were measured on an automated Sieverts instrument PCTPro-2000 equipped with a high-temperature high-pressure autoclave. A 1.1933 g quantity of freshly prepared as-cast La_3Pd_5Si sample was ground to a fine powder and enclosed into the sample holder. After the air evacuation for 1 h, the autoclave was kept at 550 K for 2 h, and then small precisely measured portions of hydrogen were added. An absorption P−C curve was obtained by measuring the equilibrium pressure in the system after the absorption of each portion at a constant temperature of 550 K. The measured data were corrected for gas temperature using the IGORPRO 5 software. The pressure-composition isotherm in the range of 0−14 bar and 0−5 H/f.u., measured during the hydrogen absorption, is shown in Figure 1. These results confirm the previous observations concerning the low-pressure phases in the $La_3Pd_5Si-H_2$ system. The α-solid solution of hydrogen in the alloy structure extends up to ~2 H/f.u. This range is slightly bigger than the one obtained from the *ex-situ* diffraction on the saturated α-deuteride (1.44(3) D/f.u.), but corresponds to the maximum possible H(D) content in this phase, if the H(D) site would be fully occupied. The composition of the lower end of the β-phase according to the P−C plot is at ~3.5−3.6 H/f.u. which correspond to the results of the structure refinements from the neutron diffraction data (3.47(2) D/f.u.). The plateau pressure of the $\alpha + \beta$ two-phase region is at ~6 bar.

PCT measurements of the hydrogen desorption reveal complete hydrogen release at 550 K. Reversible hydrogen absorption and desorption was also confirmed by the fact that hydrogenated samples were desorbing hydrogen even at room temperature by keeping them in air during a few days. X-ray powder diffraction patterns collected on the spontaneously desorbed samples showed the presence of the phase with lattice parameters similar to those of hydrogen-free La_3Pd_5Si.

Results

Phase Relations. *In-situ* neutron powder diffraction (NPD) experiments were performed on the deuteride system $La_3Pd_5Si-D_2$ at various temperatures and pressures. Three phases were identified: an α-phase (solid solution of deuterium in the alloy structure), a β-phase stable within a range of hydrogen concentrations, and a deuterium-rich γ-phase. The existence of α- and β-phases and a two-phase region between them were confirmed by PCT experiments on $La_3Pd_5Si-H_2$ system at 550 K and by *in-situ* NPD on the $La_3Pd_5Si-D_2$ system at 560 K. The detection of a two-phase region between the α- and β-phases showed that the transition is of the 1st order. To determine the cell parameters and deuterium content at the corresponding phase limits of these phases, the high-resolution synchrotron and neutron powder diffraction patterns were collected *ex-situ* at room temperature on the two-phase samples containing the α- and β-phases. The D-rich limit of the α-phase at 293 K is $La_3Pd_5SiD_{\sim 1.6}$ and the D-poor limit of the β-phase is $La_3Pd_5SiD_{\sim 2.3}$. As expected, the compositions and the corresponding cell parameters obtained from the *in-situ* NPD experiments differ slightly from those obtained from the structures refinements from the *ex-situ* NPD data at room temperature. The two-phase region between the β- and the high-pressure γ-phase was clearly visible in the *in-situ* NPD experiment. Its composition, determined from *ex-situ* NPD at 125 K, is $La_3Pd_5SiD_{4.67(7)}$. This phase has not been observed in our PCT measurements conducted only up to 14 bar because of the high pressure required for its formation (~75 bar D_2).

Cell Parameters. As shown in Figure 2, the unit cell parameters of α-$La_3Pd_5SiD_x$ increase regularly with the unit cell volume V. Expansion along a (1.4%) and b (1.5%) is bigger than along c (0.5%), and the volume increases by ~3.5%. On the $\alpha \rightarrow \beta$ transition the cell contracts along a (−3.3%) and expands along two other directions (1.3% along b and 7.9% along c) while the cell volume increases by 5.7% (comparing the results derived from *ex-situ* high-resolution neutron diffraction). This trend continues over the whole concentration range of the β-phase. Upon the $\beta \rightarrow \gamma$ transition the symmetry of the deuteride structure lowers from *Imma* to *Pmnb*, leading to a tripling of the cell parameters b and V. The cell contracts along c (−2.4%, compared to the higher end of the β-deuteride) and expands along the two other directions (1.9% along a and 2.5% along b), while the cell volume increases by 2.8%.

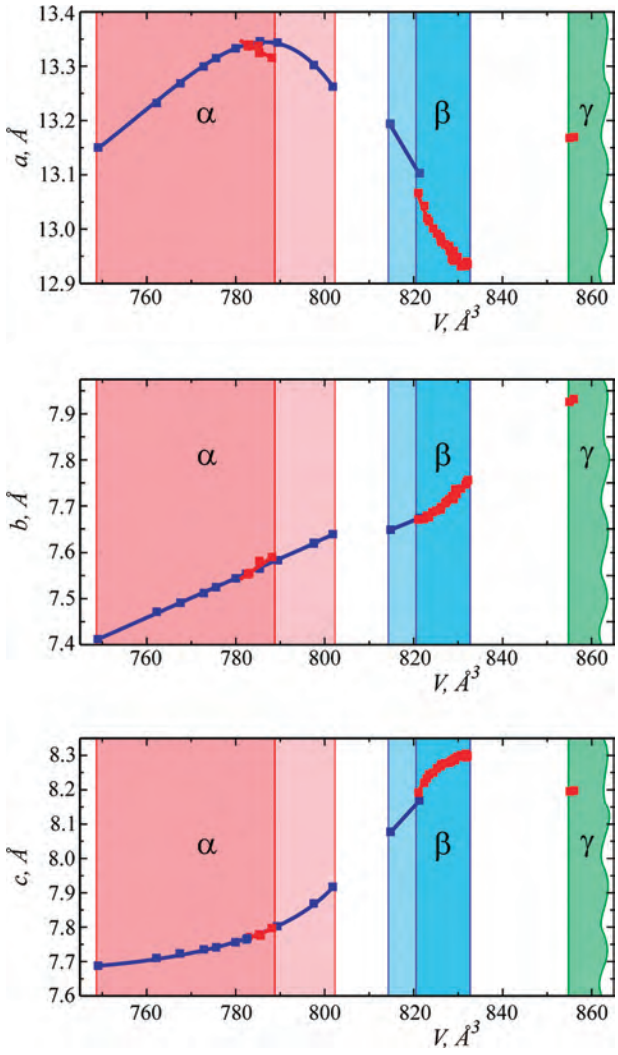

Figure 2. Lattice parameters versus the unit cell volume for different $La_3Pd_5SiD_x$ phases; data obtained upon desorption are shown by red squares and lines, absorption-in blue. The cell setting for the γ-phase was reduced to allow for direct comparison. White areas indicate two-phase regions.

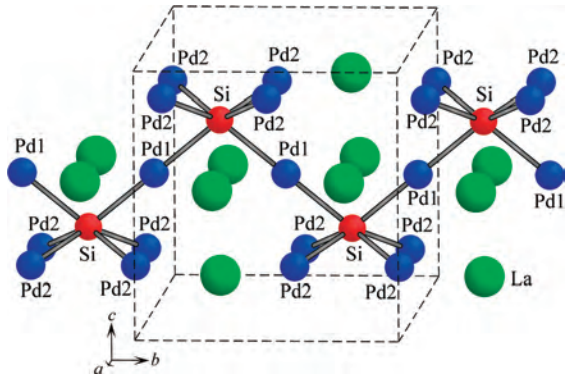

Figure 3. *Zig-zag* columns formed by Si-centered trigonal (Pd_6) prisms in the structure of La_3Pd_5Si. The unit cell is shown by dotted lines.

Structural Evolution during Deuteration. As shown in Figure 3, the structure of deuterium-free La_3Pd_5Si is characterized by Si-centered trigonal Pd_6 prisms that form *zig-zag* columns running along orthorhombic *b*. The prisms are made up by two types of transition (T) metals of which one has two Si ligands (Pd1, called bridging T metal) and the other one (Pd2, called terminal T metal) has one Si neighbor. The Pd−Si interactions appear to be rather strong as suggested by Pd−Si distances that are close to the sum of covalent radii (r_{Pd} = 1.28 Å, r_{Si} = 1.17 Å).[13] Those involving the bridging T metal (d_{Pd1-Si} ∼ 2.44 Å) are shorter than those involving the terminal T metal (d_{Pd2-Si} ∼ 2.52 Å).

As expected for a structure of this complexity, a large spectrum of metal interstices is available for deuterium occupancy, but because of various reasons (see below) only a small fraction of them is actually occupied. The occupied interstices and their non-occupied counterparts in the various phases are represented in Figure 4. Four types of interstices are occupied by D-atoms in at least one of the α-, β-, or γ-deuteride structures. Their unoccupied counterparts are denoted correspondingly □1-□4. The lower index is to distinguish symmetry nonequivalent interstices in the γ-$La_3Pd_5SiD_{4.67(7)}$. The structural evolution of $La_3Pd_5SiD_x$ compounds as a function of deuterium content can be described as follows (list of corresponding deuterium-metal bond distances for both occupied and non-occupied D sites is given in Table 2).

α-Phase. Initial deuteration leads to the occupancy of one interstitial site (D1). It has deformed tetrahedral metal coordination La_2Pd_2 and is filled at ∼72%, corresponding to the upper phase limit α-$La_3Pd_5SiD_{1.44(3)}$ (from neutron diffraction data obtained at room temperature under ambient pressure). Full occupancy of this site would correspond to the composition $La_3Pd_5SiD_2$, which is consistent with the results of the PCT measurement during absorption at 550 K under 6 bar of H_2 (Figure 1). As shown in Figure 5, the D atoms are bridging pairs of Pd atoms, thus forming isolated, non-linear 3-membered [Pd−D−Pd] units (d_{D1-Pd2} = 1.729(4) Å, ∠Pd2−D1−Pd2 = 136.54(13)°). The terminal Pd2 atom has a D ligand while the bridging Pd1 atom has none. Interestingly, the D-atom insertion, despite being rather remote from the Si atoms (the shortest Si−D contact at 3.975(5) Å), affects the Pd−Si framework. While the Pd−Si distances decrease slightly for the terminal T atoms (d_{Pd2-Si} = 2.495(5) Å), they remain constant for the bridging T atoms (d_{Pd1-Si} = 2.441(7) Å).

***β*-Phase.** Upon further deuteration, a new type of interstice becomes occupied by D2. It has a deformed tetragonal-bipyramidal metal coordination La_4Pd_2 and is filled at ∼92%. Together with site D1 (filled at ∼82%) this leads to the composition β-$La_3Pd_5SiD_{3.47(2)}$ for the lower end of the β-phase. If both D sites were fully occupied, then the upper phase limit would be β-$La_3Pd_5SiD_4$, which is consistent with the results of the PCT measurements. Compared to the α-phase the changes in the Pd−D and Pd−Si frameworks are significant. For D1 the Pd−D bond distance in the [Pd−D−Pd] units increases by 0.04 Å (d_{D1-Pd2} = 1.766(3) Å) in agreement with the higher occupancy of this site while the bond angle decreases by 16° (∠Pd2−D1−Pd2 = 119.7(2)°). As to D2, it bridges terminal Pd2 atoms of neighboring [Pd−D−Pd] units in a nearly linear configuration (∠Pd2−D2−Pd2 = 173.2(2)°, d_{Pd2-D2} = 1.782(2) Å)

(13) Emsley, J. *The Elements*, 2nd ed.; Clarendon Press: Oxford, 1991.

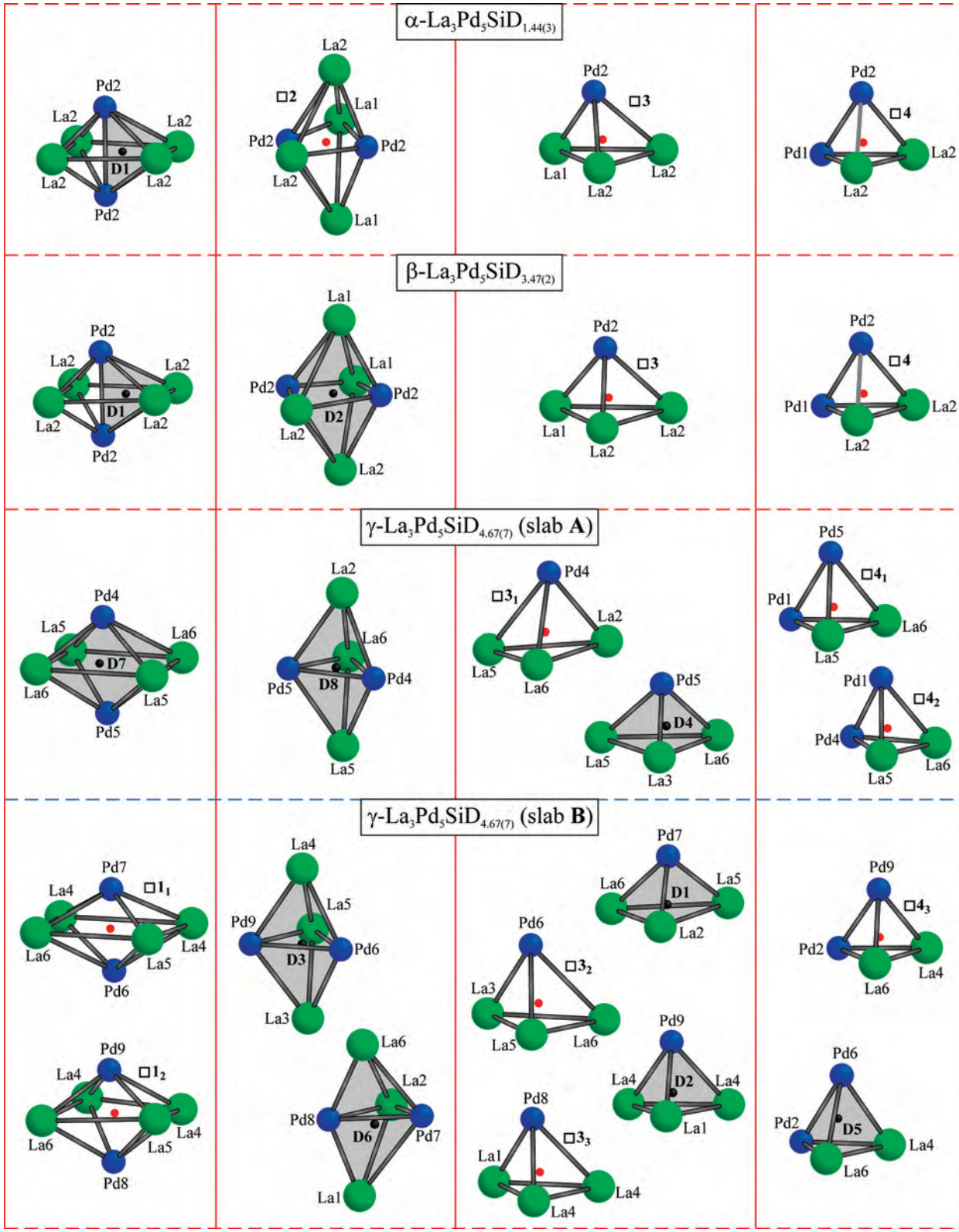

Figure 4. Occupied interstices and their non-occupied counterparts in α-$La_3Pd_5SiD_{1.44(3)}$, β-$La_3Pd_5SiD_{3.47(2)}$, and γ-$La_3Pd_5SiD_{4.67(7)}$. Occupied interstices are shadowed; the centers of non-occupied interstices are shown as red spheres. Corresponding D−M and □−M (M = La, Pd) distances are listed in Table 2.

such that these units become connected to infinite Pd−D *zig-zag* chains (−Pd2−D1−Pd2−D2−Pd2−D1−Pd2−D2−) running along *c*, that is, perpendicular to the *zig-zag* columns of Si-centered trigonal Pd_6 prisms with which they intersect via terminal T atoms (Figure 5). Similar to the α-phase the terminal T atom (Pd2) has D ligands (D1, D2) while the bridging T atom (Pd1) has none. Again, the D insertion occurs relatively far away from the Si site (shortest Si−D contact at 3.677(4) Å) but affects the Pd−Si framework significantly.

Table 2. D−M and □−M (M = La, Pd) Distances (Å) in Occupied Interstices and Their Non-Occupied Counterparts[a] in α-$La_3Pd_5SiD_{1.44(3)}$, β-$La_3Pd_5SiD_{3.47(2)}$, and γ-$La_3Pd_5SiD_{4.67(7)}$ (Shown in Figure 5)

	interstices					
compound	tetrahedral **La_2Pd_2** / tetragonal bipyramidal **La_4Pd_2**	tetragonal bipyramidal **La_4Pd_2** / trigonal bipyramidal **La_3Pd_2**	tetrahedral **La_3Pd**		tetrahedral **La_2Pd_2**	
α-$La_3Pd_5SiD_{1.44(3)}$	**D1**-2Pd2: 1.729(5)	□**2**-2Pd2: 1.496(5)	□**3**-Pd2: 1.741(5)		□**4**-Pd2: 1.832(5)	
	D1-2La2: 2.519(6)	□**2**-2La2: 2.795(3)	□**3**-La1: 2.279(2)		□**4**-Pd1: 2.891(1)	
		□**2**-2La1: 2.857(2)	□**3**-La2: 2.315(4)		□**4**-La2: 2.125(2)	
			□**3**-La2: 2.426(4)		□**4**-La2: 2.227(2)	
β-$La_3Pd_5SiD_{3.47(2)}$	**D1**-2Pd2: 1.766(3)	**D2**-2Pd2: 1.782(2)	□**3**-Pd2: 1.792(2)		□**4**-Pd1: 1.842(1)	
	D1-2La2: 2.508(4)	**D2**-2La1: 2.764(3)	□**3**-La1: 2.313(1)		□**4**-Pd2: 2.852(2)	
		D2-2La2: 2.776(4)	□**3**-La2: 2.425(2)		□**4**-La2: 2.142(1)	
			□**3**-La2: 2.493(2)		□**4**-La2: 2.254(1)	
γ-$La_3Pd_5SiD_{4.67(7)}$ (slab **A**)	**D7**-Pd4: 1.77(3) **D7**-Pd5: 1.91(3) **D7**-La6: 2.41(3) **D7**-La5: 2.81(3) **D7**-La5: 3.04(3) **D7**-La6: 3.39(3)	**D8**-Pd5: 1.71(4) **D8**-Pd4: 2.00(4) **D8**-La6: 2.39(3) **D8**-La2: 2.82(3) **D8**-La5: 2.82(3)	□$\mathbf{3_1}$-Pd4: 2.12(2) □$\mathbf{3_1}$-La2: 2.333(11) □$\mathbf{3_1}$-La6: 2.508(16) □$\mathbf{3_1}$-La5: 2.621(16)	**D4**-Pd5: 1.71(2) **D4**-La6: 2.31(3) **D4**-La3: 2.46(2) **D4**-La5: 2.56(3)	□$\mathbf{4_1}$-Pd1: 1.904(9) □$\mathbf{4_1}$-Pd5: 2.959(16) □$\mathbf{4_1}$-La5: 2.256(16) □$\mathbf{4_1}$-La6: 2.284(17)	□$\mathbf{4_2}$-Pd1: 1.846(8) □$\mathbf{4_2}$-Pd4: 2.92(2) □$\mathbf{4_2}$-La6: 2.123(16) □$\mathbf{4_2}$-La5: 2.443(16)
γ-$La_3Pd_5SiD_{4.67(7)}$ (slab **B**)	□$\mathbf{1_1}$-Pd7: 1.431(19) □$\mathbf{1_1}$-Pd6: 1.75(2) □$\mathbf{1_1}$-La5: 2.990(17) □$\mathbf{1_1}$-La6: 3.027(17) □$\mathbf{1_1}$-La4: 3.054(14) □$\mathbf{1_1}$-La4: 3.127(14)	**D3**-Pd6: 1.84(3) **D3**-Pd9: 1.87(3) **D3**-La5: 2.59(3) **D3**-La3: 2.70(3) **D3**-La4: 2.81(3)	□$\mathbf{3_2}$-Pd6: 2.109(17) □$\mathbf{3_2}$-La3: 2.235(11) □$\mathbf{3_2}$-La5: 2.494(16) □$\mathbf{3_2}$-La6: 2.624(16)	**D1**-Pd7: 1.88(3) **D1**-La6: 2.29(3) **D1**-La5: 2.44(3) **D1**-La2: 2.48(2)	□$\mathbf{4_3}$-Pd9: 1.78(2) □$\mathbf{4_3}$-Pd2: 2.920(9) □$\mathbf{4_3}$-La4: 2.283(16) □$\mathbf{4_3}$-La6: 2.352(17)	**D5**-Pd6: 1.62(2) **D5**-Pd2: 2.149(19) **D5**-La6: 2.47(2) **D5**-La4: 2.54(2)
	□$\mathbf{1_2}$-Pd9: 1.63(2) □$\mathbf{1_2}$-Pd8: 1.76(2) □$\mathbf{1_2}$-La4: 2.745(15) □$\mathbf{1_2}$-La6: 2.823(17) □$\mathbf{1_2}$-La5: 2.863(17) □$\mathbf{1_2}$-La4: 2.924(15)	**D6**-Pd8: 1.71(2) **D6**-Pd7: 1.72(3) **D6**-La1: 2.66(3) **D6**-La2: 2.74(3) **D6**-La6: 2.94(3)	□$\mathbf{3_3}$-Pd8: 1.927(19) □$\mathbf{3_3}$-La1: 2.222(9) □$\mathbf{3_3}$-La4: 2.244(13) □$\mathbf{3_3}$-La4: 2.449(14)	**D2**-Pd9: 1.91(3) **D2**-La4: 2.26(3) **D2**-La4: 2.27(3) **D2**-La1: 2.34(3)		

[a] The centers of non-occupied interstices are designated by □.

While the Pd−Si distances decrease for the terminal T atoms, that is, those having D ligands (d_{Pd2-Si} = 2.425(3) Å), they increase for the bridging Pd atoms, that is, those having no D ligand (d_{Pd1-Si} = 2.510(4) Å). These changes correlate with the anomalies in the cell parameters. The relatively strong cell expansion along *c* (7.9%) is directed along the newly formed Pd−D *zig-zag* chains, the weak expansion along *b* (1.3%) is directed parallel to the Pd−Si *zig-zag* chains, and the relatively strong contraction along *a* (−3.3%) is directed perpendicular to both the Pd−D *zig-zag* chains and the bridging Pd−Si *zig-zag* chains. No short D−D contacts (<2 Å) occur.

γ-Phase. Further deuteration leads to the β → γ transition with a symmetry lowering, which induces splitting of the structure into two types of slabs, **A** and **B**, having an abundance ratio **A/B** = 1/2 (Figure 5). Interestingly, among six available sites (see corresponding sites in Figure 4) only four remain occupied (D7 and D8 in slab **A**, D3 and D6 in slab **B**) while four new D sites with tetrahedral metal coordination become available (D4 in slab **A**; D1, D2, and D5 in slab **B**). The occupancies range between 71% (D2) and 100% (D5), corresponding to the refined composition γ-$La_3Pd_5SiD_{4.67(7)}$. The full occupancy of all sites would correspond to the composition $La_3Pd_5SiD_{5.33}$ (upper phase limit) which, however, was not reached in the PCT measurement. Consequently, the connectivity of the Pd−D network differs significantly from that in the β-phase. While slab **A** (Figure 5) contains infinite −Pd−D− *zig-zag* chains as the β-phase, but with an additional D ligand (D4) attached to a bridging T metal (Pd5), slabs **B** contain isolated 5-membered [D5−Pd6−D3−Pd9−D2] and 4-membered [D1−Pd7−D6−Pd8] fragments that derive from the −Pd−D− *zig-zag* chains in the β-phase by depopulation of 2/3 of D1 (see empty sites □$\mathbf{1_1}$ and □$\mathbf{1_2}$ in Figure 4, and corresponding occupied site D7 in slab **A**) and by attaching additional D ligands (D1, D2) to T metal sites as in slab **A**, including one (D5) that is not present in slab **A** (nor in the β-phase). Thus, the γ-phase contains both bridging T metal ligands (D7, D8 in slab **A**; D3, D6 in slab **B**) as in the β-phase, and terminal T metal ligands (D4 in slab **A**; D1, D2, and D5 in slab **B**) not present in the β-phase.

The most likely reasons for the depopulation of D sites in slab **B**, and the contraction of the interstices, are the onset of repulsive D−D interactions due to newly created sites such as D1 and D2. As expected, the changes in metal substructure induced by the fragmentation of the −Pd−D− *zig-zag* chains are substantial. Firstly, the metal coordination around D7 (slab **A**) is no longer tetrahedral as around D1 in

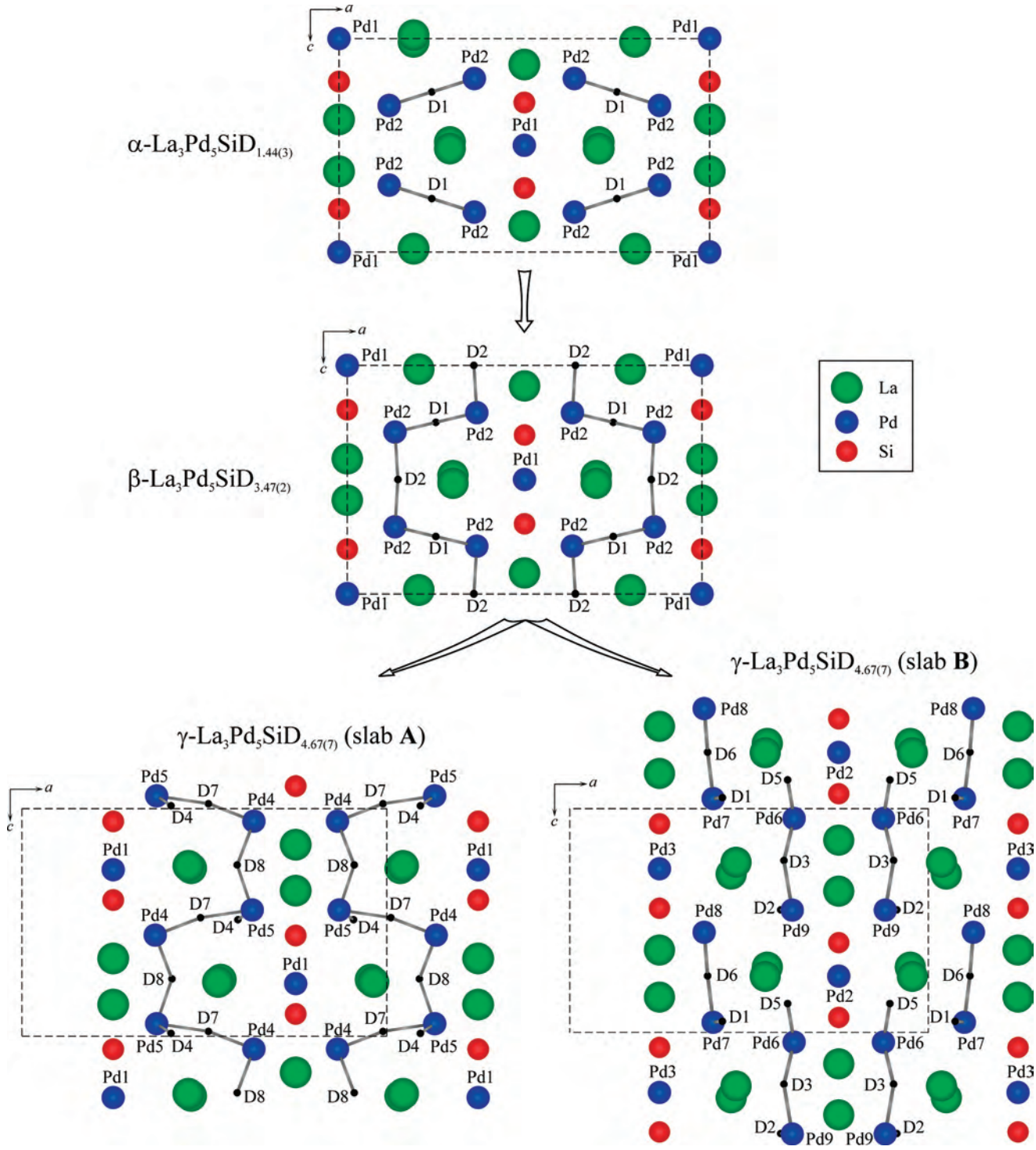

Figure 5. Unit cell projections on *ac* plane of α-$La_3Pd_5SiD_{1.44(3)}$, *β*-$La_3Pd_5SiD_{3.47(4)}$, and *γ*-$La_3Pd_5SiD_{4.67(7)}$ ($y = 0.65-0.85$ for slab **A** and $y = 0-0.15$ for slab **B**).

the *β*-phase, but deformed tetragonal bipyramidal La_4Pd_2. This is presumably due to repulsive interactions between D7 and other newly created D atom sites such as D4, which would be only ∼1.4 Å away from D7 if the latter had tetrahedral coordination such as D1 in the *β*-phase. The repulsions lead to an opening of the Pd−D−Pd bond angle such that D7 has a nearly linear Pd−D−Pd configuration (∠Pd4−D7−Pd5 = 167.44(16)°) and comes close to two more La neighbors. Secondly, the metal coordinations around D8 (slab **A**) and D3 and D6 (slab **B**) are no longer tetragonal-bipyramidal La_4Pd_2 as around D2 in the *β*-phase but trigonal bipyramidal La_3Pd_2. These changes cannot be attributed to repulsive D−D interactions (D−D > 2.1 Å) but may be due to an energy gain obtained by shortening one of the three D−La bonds (D8−La6, D3−La5, D6−La1) at the expense of the three others. Thirdly, a new interstitial site becomes available for D occupation in slab **B** (D5), in contrast to the equivalent sites in slab **A** and in the α- and *β*-phases, which cannot be occupied because of the small size of the corresponding interstices. Similar to the *β*-phase, the terminal

Pd atoms (slab **A**: Pd4, Pd5; slab **B**: Pd6, Pd7, Pd8, Pd9) have D ligands (D3, D6, D7, D8) while the bridging Pd atoms (slab **A**: Pd1; slab **B**: Pd2, Pd3) do not. Compared to the β-phase, the deuterium insertion occurs somewhat closer to the Si sites (shortest Si−D contact ∼3.0 Å) and thus affects the Pd−Si framework more strongly. The −Pd−Si− *zig-zag* chains made up by the bridging T atoms, for example, are distorted, and the Pd−Si bond distances for both terminal T atoms (those having many D ligands) and bridging T atoms (those having no D ligands) scatter over a wide range, although the former tend to be longer on average than the latter. As to the changes in cell parameters, correlations with D atom occupancies are more difficult to be established, except for the anomalous contraction along *c* that appears to coincide with the brake up of the −Pd−D− *zig-zag* chains in slab **B**.

Discussion

The reaction of La_3Pd_5Si with hydrogen is a rather complex process dominated by various competing interactions. While the metal−hydrogen (La-D, Pd−D), metal−metal (La−Pd), and metal−silicon (La−Si, Pd−Si) interactions are clearly attractive, the nonmetal−hydrogen interactions (D−D, Si−D) are not. The shortest La−D bonds in $La_3Pd_5SiD_x$ (2.52 Å in the α-phase, 2.51−2.76 Å in the β-phase, 2.26−2.66 Å in the γ-phase) are close to those in the binary deuteride LaD_{2+x} (2.43−2.60 Å)[14] while the shortest Pd−D bonds (1.73 Å in the three-member [Pd−D−Pd] fragments of the α-phase, 1.77 Å in the −Pd−D−Pd−D− *zig-zag* chains of the β-phase, 1.62 Å in the four-member [D−Pd−D−Pd] and five-member [D−Pd−D−Pd−D] fragments of the γ-phase) are similar to those in complex palladates (1.60−1.70 Å in linear $[PdD_2]^{2-}$, triangular $[PdD_3]^{3-}$, square planar $[PdD_4]^{2-}$ or tetrahedral $[PdD_4]^{2-}$ complexes).[15] Similar to the latter, the Pd−D bonds in $La_3Pd_5SiD_x$ are presumably stabilized by charge transfer from the more electropositive metal atoms (La), but their electron requirements are not obvious.

Very similar structural changes upon hydrogenation were reported for another rare-earth transition metal *p*-element compound, $LaNi_3B$.[16] Similar to γ-$La_3Pd_5SiH_x$, the hydrogenated product $LaNi_3BH_{\sim 3}$ shows a superstructure (fourfold) compared to the parent intermetallic. Likewise, hydrogenation of $LaNi_3B$ is also accompanied by an anisotropic expansion of the unit cell, including contraction in one direction, and the structure of the hydride segregates into hydrogen-free slabs containing the *p*-element (boron) and hydrogen-rich slabs containing transition metal−hydrogen fragments. Hydrogen atoms are localized in nearly fully occupied sites, and this was shown to be the result of repulsive interactions between hydrogen and boron atoms. Localization of H-atoms close to the transition metal atoms was described in terms of two-dimensional $[NiH]^-$ slabs and the limiting ionic formula $La^{3+}B^0[Ni_3H_3]^{3-}$. Formation of two-dimensional $[NiH]^-$ complexes in $LaNi_3BH_3$, counterbalanced by La^{3+} cations, was later confirmed theoretically.[17] The most important common feature of $La_3Pd_5Si-H_2$ and $LaNi_3B-H_2$ systems is the fact that a small amount of *p*-element stabilizes the ternary intermetallic phases with new structures, which do not exist in the binary rare-earth transition metal systems. Somewhat unexpectedly, the small amount of boron or silicon does not prevent H-insertion into the alloy structure, although it is likely to destabilize the hydrides since both systems are fully reversible.

Interestingly, the hydrogen filling of the La_3Pd_5Si host structure proceeds unevenly with respect to both the hydrogen content and the unit cell volume (see Figure 2). While the occupancies of the D sites in the α- and β-phases appear to increase gradually, some occupancies decrease in the more hydrogen-rich γ-phase. This is particularly true for some D sites in the −Pd−D−Pd−D− *zig-zag* chains of the β-phase (those initially occupied in the [Pd−D−Pd] fragments of the α-phase) that are no longer occupied in the γ-phase. The D site depopulation leads to a partial interruption of the infinite *zig-zag* chains and the formation of isolated [D−Pd−D−Pd] and [D−Pd−D−Pd−D] fragments. Hydrogen site depopulation at increasing hydrogen contents is a relatively rare phenomenon in solid state metal hydrides. Known cases include $Ho_6Fe_{23}D_x$,[18] ErT_3D_x (T = Ni,Co),[19] and $LaMgNi_4D_x$[20] in which deuterium occupies the centers of Ho_6 octahedra, ErT_3 and Ni_4 tetrahedra, respectively, at low D contents and leaves these interstices at higher D contents. This presumably is due to the onset of repulsive interactions between H atoms. Likewise, the depopulation of hydrogen sites in the present system can be attributed at least partially to the onset of repulsive Si−D and D−D interactions that divide the structure into Si-poor slabs that absorb hydrogen, and Si-rich slabs that do not.

Evidence for repulsive Si−H interactions in the La_3Pd_5Si-H system and in other *d*-metal silicide-hydrogen systems comes from a study of the Si−D distances in deuterides. As shown in Table 3 the shortest Si−D distances in the La_3Pd_5Si-D system are in the range 3.0−4.0 Å. They decrease with increasing D content and are comparable to those reported in other structurally characterized *d*-metal silicides such as $Ti_5Si_3D_{0.9}$ (3.23 Å),[21] $Pd_9Si_2D_{0.22}$ (3.02 Å),[2,3] $Nb_4Co_{0.9}Si_{0.1}D_{2.5}$ and $Nb_4Ni_{0.8}Si_{0.2}D_{2.7}$ (2.57 Å),[22] and $CeNiSiD_{1.2}$ (2.02 Å).[23] However, most of the systems investigated display relatively low D site occupancies (e.g., $CeNiSiD_{1.2}$) and/or atomic disorder (e.g., $Nb_4Co_{0.9}Si_{0.1}D_{2.5}$), thus rendering the reported Si−D distances less reliable. In $CeNiSiD_{1.2}$, for example, only 22% of the D site close to Si

(14) Fischer, P.; Hälg, W.; Schlapbach, L.; Yvon, K. *J. Less-Common Met.* **1978**, *60*, 1–9.
(15) Yvon, K.; Renaudin, G. In *Encycl. Inorg. Chem.*, 2nd ed.; King, R. B., Ed.; Wiley: Hoboken, NJ, 2005; Vol. *III*, pp 1814−1846.
(16) Filinchuk, Y. E.; Yvon, K. *Inorg. Chem.* **2005**, *44*, 4398–4406.
(17) Orgaz, E.; Aburto, A. *J. Chem. Phys.* **2006**, *125* (1−5), 44708.
(18) Rhyne, J. J.; Hardman-Rhyne, K.; Smith, H. K.; Wallace, W. E. *J. Less-Common Met.* **1983**, *94*, 95–105.
(19) (a) Filinchuk, Y. E.; Yvon, K. *J. Alloys Compd.* **2005**, *404−406*, 89–94. (b) Filinchuk, Y. E.; Yvon, K. *J. Solid State Chem.* **2006**, *179*, 1041–1052.
(20) Chotard, J.-N. University of Geneva, personal communication.
(21) Kajitani, T.; Kawase, T.; Zamada, K.; Hirabazashi, M. *Trans. Jap. Inst. Met.* **1986**, *27*, 639–647.
(22) Vennström, M.; Andersson, Y. *J. Alloys Compd.* **2004**, *364*, 141–145.
(23) Pasturel, M.; Weill, F.; Bourée, F.; Bobet, J.-L.; Chevalier, B. *J. Alloys Compd.* **2005**, *397*, 17–22.

Table 3. Local D Atom Environments, Shortest Si−D Distances, and Corresponding D Site Occupancies in Deuterated Transition Metal−Silicon Systems

compound	local D atom environment	shortest Si−D distances, Å	occupancy of D atom site[a]	ref.
α-$La_3Pd_5SiD_{1.44}$	La_2Pd_2	3.98	0.72	this work
β-$La_3Pd_5SiD_{3.47}$	La_4Pd_2	3.68	0.92	this work
γ-$La_3Pd_5SiD_{4.67}$	La_2Pd_2	3.00	1.0	this work
$Ti_5Si_3D_{0.9}$	Ti_6	3.23	0.09	21
$Pd_9Si_2D_{0.22}$	Pd_5	3.02[b]	0.22	2, 3
$Nb_4Co_{0.9}Si_{0.1}D_{2.5}$	Nb_4	2.57[c]	0.12	22
$Nb_4Ni_{0.8}Si_{0.2}D_{2.7}$	Nb_4	2.57[c]	0.19	22
$CeNiSiD_{1.2}$	Ce_3Si_2	2.02	0.27	23
$TbNiSiD_{1.78}$	Tb_3Ni	2.37	0.89	24

[a] Refers to the D site closest to Si site. [b] Refers to dynamically disordered D site. [c] Refers to disordered Si/T site with occupancy ratios Si/T=56/44 (T=Co) and 62/38 (T=Ni).

is occupied which favors local atomic relaxations while in $Nb_4Co_{0.9}Si_{0.1}D_{2.5}$ the reported Si−D distance refers to an average between Si−D and Co−D bonds.

The shortest Si−D distance involving an almost fully occupied D site is that reported for $TbNiSiD_{1.78}$ (d_{Si-D} = 2.37 Å, D site occupancy = 0.89).[24] Its structure is made up by columns of trigonal terbium prisms that are centered alternatively by Si and Ni atoms along the column axis. The observed displacements of the D atoms away from the triangular prism faces towards the nearest Ni atoms (d_{Ni-D} = 1.62 Å) can be taken as further evidence for the interplay between attractive metal−hydrogen and repulsive silicon−hydrogen interactions in these sorts of compounds. Taken together, the Si−D distances reported for deuterated *d*-metal silicides exceed by far those in silanes (d_{Si-H} = 1.48 Å).[25] The repulsive nature of Si−H interactions was also well illustrated in the hydrides of some ternary CeFeSi-type transition metal silicides. Thus, the hydrogenation of CeCoSi,[26] CeFeSi,[27] and CeRuSi[28] causes a pronounced anisotropic expansion of the unit cell (the *a* parameter decreases by 0.4−2.3% whereas the *c* parameter increases by 9−15%) and a strong displacement of Si atom along the *c* axis. Because the closest contact between Si and H-atoms exists only along the *c* axis, these observations suggest the H-atoms insertion into Ce_4 pseudo-tetrahedral sites (2*b*) and repulsive interaction Si−H. This interpretation was supported by structural investigations of the CeCoGeD deuteride having the same CeFeSi-type metal substructure,[27] band structure calculations,[26] and change of some physical properties[29] in the CeCoSi-H system. As to the D−D contacts in $La_3Pd_5SiD_x$ phases, they generally decrease as a function of D content (3.28 Å in α-phase, 2.54−2.93 Å in β-phase, 2.31−2.88 Å in γ-phase), but never fall below 2.1 Å. Thus, the D−D interactions can be assumed to be repulsive like in the great majority of solid state metal hydrides known so far.

Concerning the metal−metal and metal−silicon interactions, the changes induced by the different connectivity of the Pd−D network in the β- and γ-phases are small but significant. Firstly, the formation of infinite −Pd−D−Pd−D− *zig-zag* chains in the β-phase and their breakup in the γ-phase correlate with cell parameter anomalies along two directions while the absence of such anomalies along the third direction correlates with a presumably stabilizing influence of −Si−Pd−Si−Pd− chains along that direction (Figure 3). Secondly, the metal−metal and metal−silicon interactions tend to be weakened by the uptake of hydrogen as can be seen from the La−Pd, La−Si, and Pd−Si distances that tend to increase with H-content (d_{La-Pd}: 2.97−2.99 Å in La_3Pd_5Si, 2.95−3.07 Å in α-phase, 3.08−3.09 Å in β-phase, 2.94−3.25 Å in γ-phase; d_{La-Si}: 3.10−3.19 Å in La_3Pd_5Si, 3.16−3.24 Å in α-phase, 3.14−3.29 Å in β-phase, 2.98−3.77 Å in γ-phase; d_{Pd-Si}: 2.44−2.52 Å in La_3Pd_5Si, 2.44−2.50 Å in α-phase, 2.43−2.51 Å in β-phase, 2.42−2.46 Å in γ-phase). However, this trend is not general as shown for example, by the Pd−Si distances involving terminal Pd atoms that tend to decrease as a function of H content (d_{Pd-Si}: 2.52 Å (La_3Pd_5Si), 2.50 Å (α-phase), 2.43 Å (β-phase), 2.42−2.45 Å (γ-phase)). As a consequence, the metal coordination around certain D sites changes significantly in size and shape, such as those in the β-phase that changes from tetrahedral (D1) to deformed tetragonal bipyramidal in the γ-phase (D7) or from tetragonal-bipyramidal (D2) to trigonal bipyramidal in the γ-phase (D8 in slab **A**; and D3 and D6 in slab **B**, see Figure 4). While the reasons for these changes are not entirely clear, repulsive Si−D and D−D interactions play an obvious role.

Conclusions

Hydrogenation of La_3Pd_5Si proceeds in a rather subtle and unexpected manner. While the environments of the H sites change relatively little as a function of hydrogen uptake, their occupancies are strongly influenced by the presence (or absence) of Si and H ligands in their neighborhood. In particular, the breakup of infinite −Pd−H−Pd−H− *zig-zag* chains at higher H contents can be attributed at least partially to the onset of repulsive Si−H and H−H interactions that divide the structure into Si-poor slabs that absorb hydrogen and Si-rich slabs that do not. The competition between silicon and hydrogen as transition metal ligands is also revealed by the fact that Pd atoms having terminal Si ligands are capable of forming Pd−H bonds, whereas Pd atoms having bridging Si ligands are not, at least under the conditions of our measurements. Finally, while no evidence for silane-like Si−H bonds in solid state *d*-metal systems is available yet, our results suggest that such bonds can possibly be stabilized at higher pressures. This will be a challenge for the future work.

Acknowledgment. This work was supported by the Swiss National Science Foundation and the Swiss Federal Office

(24) Brinks, H. W.; Yartys, V. A.; Hauback, B. C. *J. Alloys Compd.* **2001**, *322*, 160–165.
(25) Lide, D. R. *CRC Handbook of Chemistry and Physics*, 83rd ed.; CRC Press LLC: Florida, 2003.
(26) Chevalier, B.; Matar, S. F. *Phys. Rev. B.* **2004**, *70*, 174408.
(27) Chevalier, B.; Pastruel, M.; Bobet, J.-L.; Isnard, O. *Solid State Commun.* **2005**, *134*, 529–533.
(28) Chevalier, B.; Gaudin, E.; Tencé, S.; Malaman, B.; Rodriguez Fernandez, J.; André, G.; Coqblin, B. *Phys. Rev. B.* **2004**, *77*, 014414.
(29) Chevalier, B.; Matar, S. F.; Ménétrier, M.; Sanchez Marcos, J.; Rodriguez Fernandez, J. *J. Phys.: Condens. Matter.* **2006**, *18*, 6045–6056.

of Energy and has been partially performed at the Swiss Spallation Neutron Source SINQ and Material Science Beam Line at SLS, Paul Scherrer Institute (Villigen, Switzerland), and the Swiss-Norwegian Beam Lines at ESRF (Grenoble, France).

Supporting Information Available: Details of synthesis, structure refinement, positional and displacement parameters, interatomic distances from X-ray and neutron structural data (PDF). This material is available free of charge via the Internet at http://pubs.acs.org.

IC800382X